Vibrational dynamics of very high density amorphous ice studied by high-resolution x-ray spectroscopy

Michael Marek Koza,[1,*] Burkhard Geil,[2,3] Marco Scheuermann,[2] Helmut Schober,[1] Giulio Monaco,[4] and Herwig Requardt[4]
[1]*Institut Laue Langevin, 6 Rue Jules Horowitz, BP 156, 38042 Grenoble Cedex, France*
[2]*Fachbereich Physik, Technische Universität Darmstadt, D-64289 Darmstadt, Germany*
[3]*Experimentalle Physik III, Technische Universität Dortmund, D-44221 Dortmund, Germany*
[4]*European Synchrotron Radiation Facility, 6 Rue Jules Horowitz, BP 220, F-38043 Grenoble Cedex, France*
(Received 13 August 2008; published 1 December 2008)

We report results from high-resolution inelastic x-ray scattering experiments on very high density amorphous (vHDA) water ice samples. The inelastic response of the amorphous structures has been sampled with high accuracy in the momentum Q range of the first pseudo-Brillouin zone. Well distinguished crystal-like phonons have been observed, and excitations of longitudinal and transverse polarization as well as acoustic and optic character are discerned. An averaged longitudinal velocity of sound of about 4050 m/s is established, exceeding the values of high density amorphous (HDA) and low density amorphous ice modifications reported in prior studies. In general, the dynamic features observed in the homogeneous vHDA structure appear to be better resolved and distinguished than the inelastic characteristics found in the heterogeneous structure of HDA.

DOI: 10.1103/PhysRevB.78.224301 PACS number(s): 61.43.−j, 63.50.Lm, 61.05.cf, 64.70.Ja

I. INTRODUCTION

The collective vibrational dynamics of the low density amorphous (LDA) ($\rho \approx 31$ molecules/nm^3) and high density amorphous (HDA) ($\rho \approx 39$ molecules/nm^3) ice structures[1] have been extensively studied by inelastic x-ray (IXS) and neutron scattering (INS) experiments.[2–7] IXS has provided a dynamic response of the two amorphous ice modifications that can be termed crystal-like.[2,3] This attribute reflects the feature of distinguished well-defined phonon modes, which can be described in terms of collective excitations of crystalline matter as being of longitudinal and transverse polarization and of optic and acoustic character. Of course, due acknowledgment has to be taken of the disorder of the solid water samples taking influence on the dynamic features, however, leaving a distinguished dynamic characteristics reminiscent of crystalline ice structures not observed in other disordered materials before.

The crystal-like IXS response has been affirmed by the INS in which features, characteristic for glassy matter were found missing. As such high-resolution INS experiments could not establish the presence of a boson peak, i.e., an excess of vibrational modes obeying the Bose-Einstein statistics.[5–8] Beyond the consistency found within microscopic dynamics, macroscopic observables governed by collective excitations showed as well a satisfactory agreement with the IXS and INS data. Measured velocity of sound and thermal conductivity of LDA and HDA structures are mentioned here as examples.[9,10]

The observation that HDA can be annealed into an amorphous structure of even higher density, referred to as very high density amorphous ice (vHDA) ($\rho \approx 41$ molecules/nm^3)[11–13] offered the opportunity of additionally testing the crystal-like phonon hypothesis. Moreover, as it was indicated before by sampling the static structure factor in INS and IXS experiments[2,5] and evaluated in full detail later on[14–17] HDA, in contrast to LDA and vHDA, is a heterogeneous structure which can be understood as a mixture of nonidentical structural entities on a spatial scale of some nanometers. *A priori* we may expect dynamic features established in HDA to be related to, however, better distinguished in the vHDA matrix owing to its homogeneity and extreme density. This conjecture has been confirmed by INS measurements showing the lowest Debye levels in the vibrational density of states and, hence, the highest Debye temperatures in vHDA (Refs. 7 and 14) and by nuclear magnetic resonance experiments reporting the shortest spin-lattice relaxation times $\langle T_1 \rangle$ for vHDA among all amorphous ice structures.[18]

Here, we extend our observation of the microscopic dynamics of vHDA to high-resolution IXS experiments opening up the possibility of sampling Q numbers within the first pseudo-Brillouin zone. The presented results should be therefore understood as a completion of the high-resolution coherent INS results sampling Q numbers within the second and third pseudo-Brillouin zones of the amorphous ice structures.[7,19] This manuscript may be as well considered as a completion of prior IXS studies dedicated to the dynamics of LDA and HDA.[2,3] Except for the sample preparation the experimental procedure, the data evaluation and the data interpretation are, hence, well described in the preceding publications.

II. EXPERIMENT

The entire set of measurements was performed with three vHDA samples of deuterated material. Please see for a detailed description of the preparational procedure Ref. 15. One sample was prepared at the Institut Laue Langevin (ILL) in Grenoble, France at a nominal pressure of 1.5 GPa and a maximum annealing temperature of 145 K. We refer to this sample as sample 1 throughout this paper. Two samples were prepared in the physics department of the Technical University Darmstadt (TUD) in Germany at the nominal pressure of

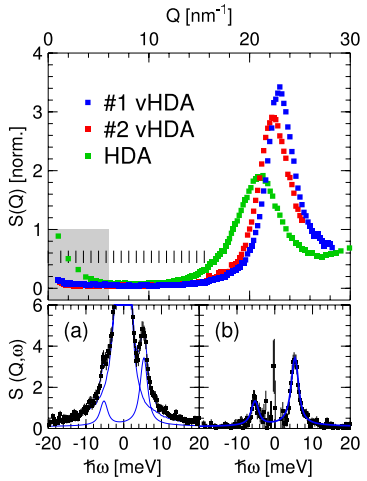

FIG. 1. (Color online) (Top) Static structure factor $S(Q)$ of the two vHDA samples reported here and the HDA sample presented in detail in Refs. 2 and 3. Gray-shaded area indicates the small-angle part of $S(Q)$ giving evidence of an intensity excess and, hence, of the heterogeneous character of the HDA structure. Small vertical lines represent the applied Q sampling. (a) Inelastic intensity of sample 1 measured at 2.00 nm^{-1}. Lines represent fits with Lorentzian lines. (b) Same spectrum as (a) with suppressed elastic line. Line with the data indicates the fit result of the pure phonon intensity convoluted with the spectrometer's resolution function.

1.1 GPa and maximum annealing temperature of 140 K. We refer to these structures as sample 2. Figure 1 reports the static structure factors $S(Q)$ of 1 and 2 as compared to HDA presented in Refs. 2 and 3. Note that for a comparative presentation the data are grossly normalized to the same integral intensity in the Q range 2–25 nm^{-1} with respect to the HDA results. The shift of the strong peak in $S(Q)$ of sample 2 toward smaller Q and its broadening is a result of the relaxed preparational conditions p and T with respect to the formation conditions of sample 1.[15]

The high-resolution x-ray spectrometer ID16 at the European Synchrotron Radiation Facility in Grenoble, France was utilized for the measurements and an experimental setup and procedure as it had been reported in prior publications was applied.[2,3] An energy resolution of about 1.6 meV full width at half maximum (FWHM) was accessed with a resolution line of Lorentzian shape. For a comprehensive presentation and discussion of the IXS data a comparison of the monitored energy-momentum ($\hbar\omega$-Q) phase space and of the resolution functions with those accessed in the inelastic neutron-scattering study of Ref. 7 is reported in Fig. 2. The phase space mapped out by the ID16 experiment complements the $\hbar\omega$-Q region covered by the neutron spectrometers IN4 and IN6 in the acoustic-phonon region $\hbar\omega \lesssim 20$ meV. Due to the kinematics of neutrons such a complete coverage of the phase space at $Q \lesssim 1$ Å^{-1}, i.e., typically within the first Brillouin zone of crystalline structures, is not achievable with INS techniques. Note that for intensity reasons the Stokes line (energy gain of sample) has been exploited at ID16. In Fig. 2 we have retained the convention applied in Ref. 7 and plot the Stokes side on negative-energy scale. Any other figures report the Stokes line on positive scale.

An accumulation of inelastic spectra was performed by subsequent repetition of energy scans (typically 3–5) at fixed

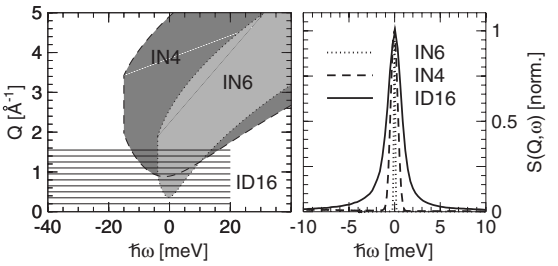

FIG. 2. Left-hand side reports the $\hbar\omega$-Q phase space coverage by the IXS spectrometer ID16 of the European Synchrotron Radiation Facility and by the neutron spectrometers IN4 and IN6 of the Institut Laue Langevin (Ref. 7). Full lines indicate the extension of energy scans recorded at ID16 in constant momentum Q mode. The Stokes line is plotted here on negative-energy scale. Figure on the right-hand side compares the resolution functions of the three spectrometers ID16 (FWHM≈1.6 meV), IN4 (FWHM≈0.8 meV), and IN6 (FWHM≈0.2 meV).

Q positions of the multianalyzer unit. For some scans at a single sample different illuminated sample volumes were chosen. Prior to and after the inelastic scans the quality of the samples was checked by monitoring $S(Q)$ as it is indicated in Fig. 1. By this procedure we could, on one hand, attest the identity of the two samples prepared at the TUD and of the signals upon illuminating different sample volumes. On the other hand, we could confirm that no beam damage had been done to the samples during any of the inelastic scans. These findings allow us to comprise all scans, according to their Q numbers and irrespective of the sample volumes illuminated, of the ILL structure and of the two TUD samples into two sets 1 and 2, respectively. Standard Q sampling applied during the study is indicated in Fig. 1 by small vertical lines. The dynamic structure factor $S(Q,\omega)$ was obtained from the raw data following established procedures and its parametrization by a suite of Lorentzian lines was followed according to prior data evaluation approaches.[2,3,19] Figure 1(a) reports a spectrum taken at $Q = 2.0$ nm^{-1} and fit results accounting for the elastic line and the phonon peak taking both, the annihilation (anti-Stokes line, negative-energy scale) and the creation (Stokes line, positive-energy scale) process, into account.

As it can be judged from Fig. 1, both vHDA 1 and 2 structure factors $S(Q)$ are featured by an even profile in the Q range 1–16 nm^{-1}. In the case of HDA the enhanced small-angle signal gives evidence of the heterogeneous character of the amorphous matrix.[14–17] This signal is of purely elastic intensity. However, due to the extensive Lorentzian-shaped energy resolution of the IXS spectrometer reported in Fig. 2 the entire low-Q region of $S(Q,\omega)$ is obscured and inelastic signal masked by the elastic line making its interpretation a challenging task.[2,3] This argument applies with even higher severity to the signal in the vicinity of the strong peak in $S(Q)$, i.e., at $Q > 12$ nm^{-1} in LDA (see Ref. 2) and at $Q > 16$ nm^{-1} in HDA and vHDA. An interpretation of acoustic phonons in amorphous ice structures is practically impossible at Q numbers exceeding the ones applied in our study. Nonetheless, in the case of vHDA samples the appreciably reduced elastic intensity at Q numbers reported here allows us to subtract the elastic resolution measured independently

with a standard scatterer from the $S(Q,\omega)$ signal of the samples and to elegantly suppress the elastic line contribution as it is indicated in Fig. 1(b).

All fits have been performed to the $S(Q,\omega)$ data for consistency with prior data evaluations. Note, that we focus in the following presentations on the difference profiles as they offer a more detailed view on the phonon line shapes. We retain, however, the designation of dynamic structure factor $S(Q,\omega)$ to the difference profiles. If not stated otherwise, all reported $S(Q,\omega)$ have been normalized to the intensity of the elastic peak.

Data of ice IX and XII are shown here as polycrystalline references. They have been adopted from Refs. 3 and 19 which describe details of sample preparation and of the experimental procedure. It is noteworthy that the preparations of ice IX and XII followed in both cases in analogy to the formation of high density amorphous structures the compression of ice I, however, either at higher temperatures $T \approx 160$ K for ice IX (Refs. 20 and 21) or higher compression rates for ice XII.[21,22] The presentation of the results has been adapted here to the presentation of the vHDA data whereby the intensity of the polycrystalline spectra has been normalized with respect to the intensity of the vHDA spectra at corresponding Q numbers.

III. RESULTS

Figures 3 and 4 report the dynamic structure factor $S(Q,\omega)$ of samples 1 and 2 in the low ($Q \leq 6.5$ nm^{-1}) and high ($7.25 \leq Q \leq 15.5$ nm^{-1}) momentum range, respectively. Similarities of the data sets recorded with the two samples are obvious. Hence, subtle differences which can be conjectured from the detectable distinctness of $S(Q)$ of samples 1 and 2 as shown in Fig. 1 are concealed by the statistics of the weaker signal in the inelastic channels of $S(Q,\omega)$.

From a qualitative inspection of the signal profiles, we may separate the results into three Q regimes in which different features become observable. At $Q \lesssim 4.25$ nm^{-1} the line shape of the inelastic response can be approximated by a single Lorentzian line. The center position of the peak follows a linear dependence upon increasing Q accompanied by an increase in the peak width. At $Q=5.0$ nm^{-1} the single peak becomes visibly distorted from a single Lorentzian line characteristics and a distinct second peak develops at momentum numbers $5.0 < Q \leq 9.5$ nm^{-1} centered at an energy of about 9 meV. This second peak does not show any obvious dispersive behavior, whereas the first one remains dispersive up to about 11 nm^{-1}, its center position taking on energies of 20–24 meV.

At even higher momentum numbers the inelastic signal takes on a profile reminiscent of the density of states $G(\omega)$ of high density amorphous ice structures.[7] This is accomplished at Q numbers above 9.5 nm^{-1}, at which in relation to the intensity of the peak at 20–24 meV emanating from the dispersive mode a boost in intensity at the low-energy 9 meV peak as well as above 24 meV is detected. Note that this intensity boost happens at Q numbers conform with the onset of the second pseudo-Brillouin zone which we interpret as the half distance $Q_M/2$ to the position $Q_M \approx 23$ nm^{-1} of the first strong peak in $S(Q)$ of vHDA (Fig. 1).

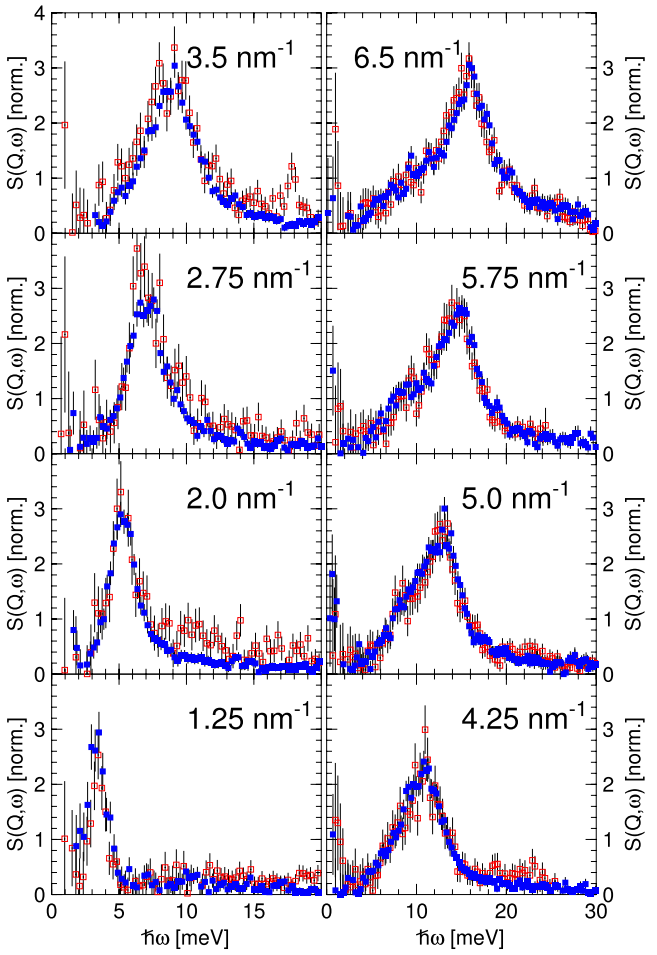

FIG. 3. (Color online) Dynamic structure factor $S(Q,\omega)$ in constant Q presentation of samples 1 (blue, full symbols) and 2 (red, empty symbols) taken at Q numbers given in the figures. Data taken at 2 nm^{-1} are multiplied by a factor of two for matching y scales. Two different x scales have been chosen for a clear presentation of the profile details. Note the dispersive character of the strong peak following grossly a linear dependence upon Q.

As we deal here with purely coherent signal this $S(Q,\omega)$ profile reminiscent of $G(\omega)$ is only a gross approximation to the real vibrational density of states. To substantiate the coherence effect within the high-Q data we have performed an incoherent approximation to the data of crystalline ice XII. A crystalline counterpart has been chosen for which the most accurate data on coherent and incoherent scattering signals are available from experiments at ID28 at the European Synchrotron Radiation Facility and at TOSCA at the ISIS neutron spallation source of the Rutherford Appleton Laboratories, respectively.[3,19] Figure 5 reports the incoherent dynamic structure factor as it has been measured at 20 K at TOSCA at ISIS and calculated from the coherent signal in the Q range 12.5–15.5 nm^{-1} for the equivalent temperature.

The comparison indicates a very good incoherent approximation within the energy range of the nondispersive peak below 20 meV. Note, for example, that the complex line shape of the strong peak and the mode gap at around 18 meV are well reproduced within the coherent data. At energies of about 24 meV the coherent signal visibly overemphasizes the

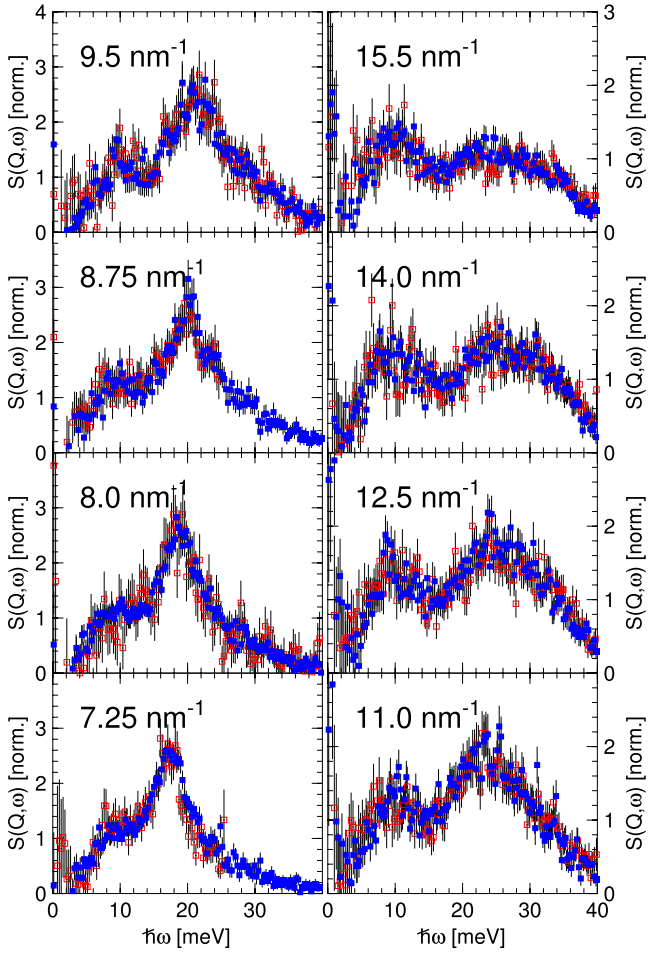

FIG. 4. (Color online) Dynamic structure factor $S(Q,\omega)$ of sample 1 (blue, full symbols) and sample 2 (red, empty symbols) in constant Q presentation. Q numbers given in the figures correspond to the vicinity of the first pseudo-Brillouin-zone boundary. Note the dispersive character of the strong peak up to energies of more than 20 meV.

peak emanating from the dispersive mode at lower Q. The phase space covered is not sufficient for a satisfactory incoherent approximation. An analogous conclusion can be hence drawn on the dynamic properties of the vHDA. The dominant peak at energies of 20–24 meV and at Q numbers as high as 15.5 nm^{-1} originates from the dispersive mode at lower Q.

Figure 6 reports parameters obtained from Lorentzian fits to the spectra whose inelastic signal can be approximately described by a single line at $Q \leq 3.5$ nm^{-1} and two lines at 4.25 nm$^{-1} \leq Q \leq 9.5$ nm^{-1}. Shown are the positions of the peaks, their full widths at half maximum Γ and the intensity in respect to the intensity of the elastic line. Note that the vertical bars plotted with the data points representing the dispersion relation correspond with and indicate the obtained Γ. Obtained reliability parameters are of the order of the data symbols. Two data sets are plotted for sample 1. The "long" data set has been measured in the entire energy range of phonons −20 meV–40 meV. The "short" data set has been restricted to the energy range of the dispersive mode −5 meV–25 meV, only. It reproduces therefore with good

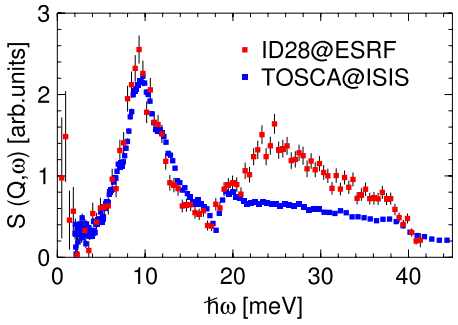

FIG. 5. (Color online) Dynamic structure factor $S(Q,\omega)$ of ice XII measured with incoherent neutron scattering at TOSCA at ISIS and coherent IXS at ID28 at ESRF (Ref. 19). IXS signal has been computed from the spectra in the vicinity of the Brillouin-zone boundary 12.5–15.5 nm^{-1}. Note the excess signal in the coherent data above 20 meV giving evidence of an incomplete incoherent approximation.

accuracy the peak position in the plotted Q range. The full width at half maximum Γ and in particular the intensity of the peaks are less reliable numbers.

The decomposition of the inelastic signal into two lines, dispersive and nondispersive, at 4.25 and 5.0 nm^{-1} tends to overestimate the separation of the assumed modes or to level out their intensities. This can be best seen with the parameters obtained with sample 1. Despite this local numerical ambivalence the energy of the nondispersing mode (9.1 ± 0.1 meV) and the average longitudinal velocity of sound (v_l=4053 ± 10 m/s) can be reliably determined from

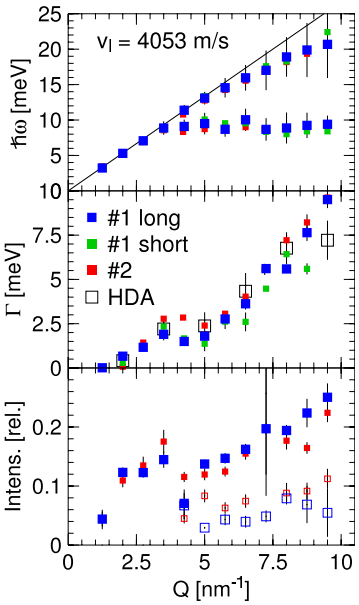

FIG. 6. (Color online) (Top) Dispersion relation $\hbar\omega(Q)$ of vHDA samples 1 and 2. Solid line reports a linear fit to the phonon dispersion in the Q range up to 3 nm^{-1}. The averaged longitudinal velocity of sound is approximated as 4053 ± 10 m/s. (Middle) Full width at half maximum $\Gamma(Q)$ of the dispersive peak of the acoustic longitudinal mode approximated by Lorentzian lines. (Bottom) Intensity of the acoustic (full symbols) and optic (open symbols) mode in relation to the elastic peak intensity.

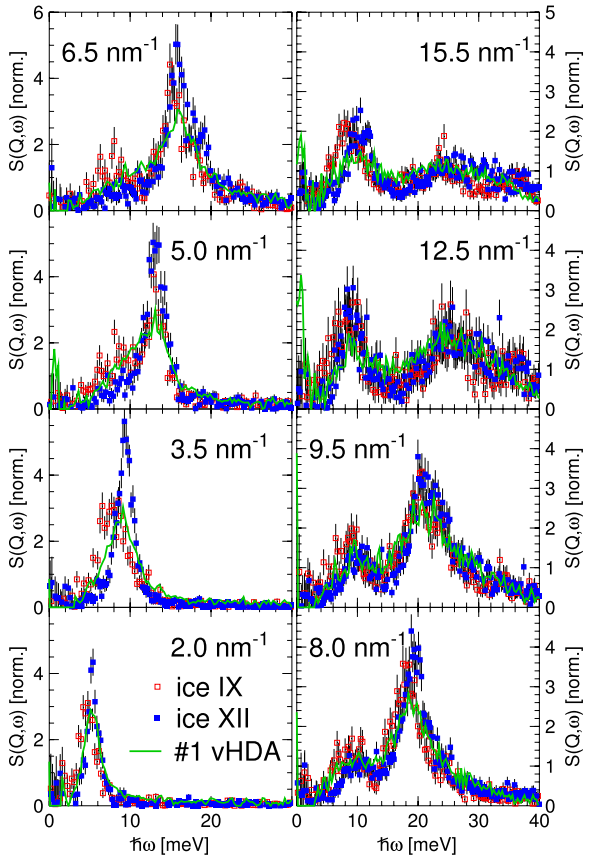

FIG. 7. (Color online) Dynamic structure factor $S(Q,\omega)$ of polycrystalline samples IX (red empty symbols) and XII (blue full symbols) and amorphous sample 1 (black solid line). Q numbers are given in the figures. Data on polycrystalline samples are adapted from Ref. 3.

fits to all data sets reported in Fig. 6. Both are clearly augmented when compared with results on HDA (7.8 ± 0.2 meV and $v_l = 3640 \pm 70$, respectively) and conform with results from inelastic neutron-scattering experiments.[3,7] When taking into account $v_l = 4053 \pm 10$ m/s, the Debye temperature obtained from neutron backscattering experiments, and approximating the density of vHDA with 41 molecules/nm^3, we obtain a transverse velocity of sound v_t of 2000 m/s. Γ numbers of HDA are as well reported with the phonon peak linewidths in Fig. 6. They match the upper values of the entire set of vHDA results.

For the readers' convenience we compare in Fig. 7 some selected spectra of ice IX and XII samples with the response of vHDA sample 1. There are two points becoming particularly obvious from this simple qualitative comparison. First of all, it is obvious that the vHDA spectra conform to the signal of the polycrystalline counterparts. The conformity comprises the properties of the dispersive phonon as well as the general variation in the spectral profile upon Q changes. Note that in the case of the crystalline materials this intensity variation is governed by complex selection rules owing to the crystals' symmetry.[23–26] In more detail, it is as well obvious that despite a slightly augmented linewidths the peak positions identified in vHDA are in closer agreement to ice XII than to ice IX peak positions. A feature anticipated by the correspondence of the vibrational density of states discussed in Ref. 7 and of the averaged longitudinal velocity of sound v_l reported in Ref. 3 as 3660 ± 130 m/s for ice IX and 4060 ± 50 m/s for ice XII, albeit, the velocity of sound data necessitate a thorough experimental cross-check for the mass effect of protonated and deuterated sample material.[6,7,9,27]

IV. DISCUSSION

It has been shown in some recent experimental studies that vHDA may be understood within the framework of amorphous ice structures as a homogeneously disordered matrix of highest density among all other disordered ice structures found so far. Correspondingly, in x-ray and neutron-scattering experiments it is characterized by extreme properties. For example, it shows the highest Q value of the first peak position in $S(Q)$ and the smallest peak width.[14,15,17,28,29] Its vibrational density of states $G(\omega)$ gives evidence of the lowest Debye level and highest energy of the predominant phonon peak both resulting in the highest Debye temperatures of all amorphous ice structures.[7,14] This observation proved to be in agreement with the temperature dependence of the Debye-Waller factor.[6]

Features established in the present study are in line with those observations. Here we have found a strongly augmented velocity of sound of the dispersive mode and the highest-energy value of the nondispersive low-energy excitation. Both are to be seen in direct relation to the response established by neutron-scattering techniques with the difference of a distinct phase space coverage. Due to the kinematic properties of x rays the inelastic response monitored here within the first pseudo-Brillouin zone at $Q < 11.5$ nm^{-1} is governed by direct-scattering processes. Applying the nomenclature established for crystalline materials we may state that the sampled momentum $\vec{Q}$ corresponds with the very momentum $\vec{q}$ of the collective mode without the contribution of a lattice vector evoking umklapp-scattering processes, i.e., $\vec{Q} = \vec{G}_{hkl} \pm \vec{q}$, with $\vec{G}_{hkl} = 0$. The information content of the data merits, hence, from comparatively simple selection rules governing the intensity of the dynamic structure factor $S(q,\omega)$.

We wish to point out two of these selection rules which are instructive for understanding the intensity evaluation upon Q variation, restricting our consideration at the beginning to crystalline structures of high symmetry. One phonon selection rule is given by the scalar interaction of the probe with the scatterers, valid for both neutrons and x rays in the energy range considered here.[23–25] This scalar interaction prohibits the detection of modes whose polarization vector is perpendicular to the phonon propagation vector, i.e., the momentum $\vec{q}$. The other selection rule is given by the averaging over pair-correlation functions within the $S(q,\omega)$ and governs the intensity of optic modes. Considering the case of $Q = q \approx 0$, averaging over a basis of identical scatterers with opposite amplitudes $(+a)$ and $(-a)$ results in null intensity. This applies to any optic mode irrespective of its polarization, longitudinal or transverse. Consequently, deep within the first Brillouin zone the probability of detecting an optic

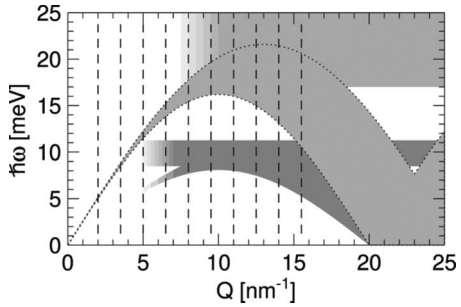

FIG. 8. Sketch of phonon dispersion in energy-momentum phase space. Indicated are the averaged longitudinal and transverse acoustic phonons and two bands of optic excitations related to the acoustic modes. The contrast increase toward higher Q numbers on the optic as well as the transverse acoustic bands indicate the scattering intensity expected from a simple inspection of phonon selection rules and approximately observed in the IXS experiment. Dashed vertical lines indicate the Q sampling by the IXS experiment. See text for details.

phonon is strongly reduced when compared to an acoustic mode characterized by in-phase moving scatterers, i.e., with the amplitudes $(+a)$ and $(+a)$. For these two reasons only a single peak is detectable at $Q \lesssim 5.0$ nm^{-1}. It is due to a dispersive mode of longitudinal polarization, i.e., the longitudinal acoustic phonon.

These strict rules are lifted when lattice vectors come into play $\vec{G}_{\mathrm{hkl}} \neq 0$ at higher Q numbers. An even more drastic perturbation is expected in disordered systems, in which the attributes of transverse and longitudinal polarization, Brillouin zones, lattice vectors, and, to some extent, acoustic and optic modes are ill defined and only applicable in an approximative way. However, note that within the high-energy band at $\hbar\omega \gtrsim 24$ meV the intensity increases visibly at Q numbers corresponding with the second pseudo-Brillouin zone as it may be expected for optic phonons. The nondispersive, hence, optic peak at 9.1 meV becomes clearly detectable at momentum numbers higher than 5 nm^{-1}, and since it is crossed by the longitudinal acoustic mode without taking any obvious influence on it, its polarization is predominantly of transverse character. We have summarized this simplified selection rule discussion in Fig. 8 in a sketch reporting the ill-defined phonon dispersion as it has been introduced in Ref. 7. Here it is decorated by optic phonons and the hypothetical detectability of the mode bands.

Another important observation connected to the applied deuterated sample material is the absence of any fingerprint of the librational band. We have shown by INS that in deuterated vHDA samples this librational band sets in at energies as low as 34 meV.[7] The missing signature of the librational band in the IXS experiment is, however, expected as the amplitudes of the librational modes are determined by the movement of the hydrogens which result in a minor contribution to the IXS cross section. The result that the here detected intensity within the vibrational region $\hbar\omega \lesssim 40$ meV complies well with any other ice sample measured with IXS shows that the coupling of librations and phonons is, if at all present, very weak leaving the phonons unperturbed. Note that the shortened energy scale of Fig. 3 is done for presentation reasons; the measured intensity is null up to energies of 40 meV, i.e., beyond the plotted region.

An obvious question concerning the phonon linewidths arises from the heterogeneous character of HDA structures[14–17] which can be judged upon from the ascending signal toward low Q numbers and the augmented linewidth of the first peak in $S(Q)$ data of Fig. 1. One might expect the phonon mean-free path and phonon lifetime to be reduced and, thus, phonon linewidths Γ to be enhanced in HDA when compared to the phonons of the homogeneous vHDA matrix. Indeed a qualitative inspection of the spectra at low Q indicates a broadening of the HDA peaks. However, no clear support can be offered by the results from the parametrization of the spectra. As it is shown in Fig. 6 the Γ of HDA tends to be at the upper value of all data estimated for the vHDA samples. In spite of the complex physics determining the intensity and line shapes of the modes, this trend is far from establishing unequivocally a phonon broadening and a reduction in mean-free path and lifetime of the longitudinal acoustic mode. Nonetheless, we may term the qualitative and quantitative observations as being conform to a scenario of reduced phonon lifetimes due to the mesoscopic structural heterogeneity of HDA.

It is important to note that the Γ computed in all amorphous ice structures LDA, HDA, and vHDA finds a correspondence with linewidths of some crystalline structure. A resemblance has been established between the inelastic response of LDA and ice I_c and the conclusion of an analogy of HDA and vHDA with ice IX and ice XII is suggestive, not excluding other high density crystalline forms. In view of the augmented longitudinal velocity of sound and of the energy of the transverse optic modes ice XII may be a better analog for vHDA. In this respect all the amorphous ice samples reflect crystal-like phonon properties.

From a qualitative comparison of the spectra with data obtained on liquid samples[30–33] a conclusion upon a resemblance of the dynamics of liquid and the amorphous water ice structures appears to be inappropriate. It is indeed by no means justified when computed parameters such as velocity of sound and phonon linewidths are considered. Note that the application of pressure augmenting the densities of liquid samples toward the ones of the high density amorphous structures results, for example, in an even more dramatic departure of the phonon linewidths of the liquids from the disordered solids.[34–36]

It is rather tempting to interpret the crystal-like phonon properties as a consequence of highly ordered local structures resembling a single or some crystalline counterparts.[37] The application of a single locally crystal-like structure may be justified for the homogeneous structures LDA and vHDA, less intuitive for HDA as an obvious mixture of distinct local structures and definitely not applicable to the strongly heterogeneous amorphous modifications intermediate with respect to HDA and LDA.[14,15]

The amazingly distinguished and characteristic inelastic response in IXS and INS experiments should be rather considered as a bench marking result for simulation and modeling approaches trying to account for the nature of the manifold of amorphous ice structures. The vibrational inelastic response is determined by the second derivatives of all the

atomic potentials underlying the formed amorphous matrix. It constitutes therefore a more stringent testing platform than any elastic response reflecting the distribution of the potential minima only. As we have shown here and in prior publications the elastic response is monitored with the inelastic signal by IXS experiments and measured simultaneously by INS.

However, if we reduce modeling efforts to molecular-dynamics (MD) simulation only the experimentally established $S(Q,\omega)$ poses a stringent requirement of a minimum box size. This applies to the experimentally established small-angle signal[17] as well as to the phonon dynamics. If we characterize the number of molecules in a simulation box by $n\times 512$, we may formulate a relation between the molecular density $\rho=N/V$ of the sample, the velocity of sound v, the simulation box size, and the minimum energy that can be calculated as $Q=2\pi[n\times 512/\rho]^{-1/3}$, $\hbar\omega_{\min}=CvQ$, $C=1/1519$ meV $(\mathrm{m/s})^{-1}$ nm. Hence, for vHDA with $\rho\approx 41$ molecules/nm^3 and a box size of 512 molecules MD results do not contain any information on the longitudinal $v_l=4050$ m/s and transverse $v_t=2000$ m/s acoustic phonons below 7.2 and 3.6 meV, respectively. For a complete calculation of the $S(Q=1.25\ \mathrm{nm}^{-1},\omega)$ a simulation box of more than 5200 molecules ($n>10$) is required, cutting off the longitudinal acoustic phonons below 3.3 meV, anyhow. To access features at 0.5 meV, which constituted a typical low-energy limit in our high-resolution time-of-flight experiments,[38] a simulation box of more than 1.5×10^6 molecules ($n>3000$) is necessary to account for the longitudinal acoustic modes correctly and without creating any correlation peak in the low-Q region of the static structure factor.[17]

Owing to the currently limited computation power we might not expect a soon response from MD simulations on such a huge number of molecules. A combined molecular and lattice dynamics approach appears to be a technique far more promising for obtaining modeled results.[39–41] Those recently published data offer, however, not only a promising perspective for modeling $S(Q,\omega)$ of amorphous ice samples but they pose some important questions concerning the reliability of modeled results. The inelastic response obtained in the energy range of acoustic phonons of HDA when compared to the results of ice I_h does not conform with any experimental results published. This holds for the density of states of HDA measured by INS at ambient pressure[5–7,19] and *in situ*,[42] and of HDA obtained as a transient product of the vHDA to LDA transformation.[14] Within the Debye framework of harmonic solids the modeled excess of $G(\omega)$ HDA over ice I_h data is not in agreement with the phonon velocity of sound determined from IXS (Refs. 2 and 3) and supersonic measurements.[9,27,43,44] The modeled data do not comply either with the Debye temperatures computed from highest-resolution neutron backscattering results.[6,7]

To be very clear at this point, this disagreement does not question the excellent quality of the studies performed, but it simply points out that the properties of the HDA structure formed by computation methods do not agree with the behavior of a real HDA sample. The reasons for this discrepancy can be manifold, e.g., size of the simulation box, thermodynamic ensemble, or potentials applied and remain to be examined. However, it is as well very clear that those reasons might have left equivalent effects in other molecular-dynamics results published in an impressive number of publications and re-examined in numerous reviews over the last few years.[45–50]

V. SUMMARY AND CONCLUSIONS

We have applied high-resolution inelastic x-ray spectroscopy to study phonon properties of very high density amorphous ice structures with a focus on the first pseudo-Brillouin zone. The dispersion of a longitudinal acoustic mode with an averaged velocity of sound of ≈ 4050 m/s has been established. An averaged eigenvector of this mode is detectable up to energies of 22 meV. In analogy to the response of LDA and HDA another nondispersive mode has been observed with an approximated energy of 9.1 meV. This mode becomes detectable at Q numbers higher than 5 nm^{-1} marking its character as transverse optic.

In accordance to the density of vHDA ≈ 41 molecules/nm^{-1} higher than the density of HDA ≈ 39 molecules/nm^{-1} the quantified numbers tend toward more extreme values than those established in HDA. Moreover, in accordance to the pronounced homogeneity of the vHDA matrix all dynamic features appear to be more distinctly distinguished than those found in the heterogeneous structure of HDA. The observed features are in full agreement with inelastic neutron-scattering results on very high density amorphous ice modifications established, however, within the second and third pseudo-Brillouin zone.[7]

The entire set of INS and IXS experimental data covers hence a Q range of three pseudo-Brillouin zones (1.25–50 nm^{-1}) and the entire energy range of collective translational modes (0–40 meV). Since the sampled coherent dynamic structure factor $S(Q,\omega)$ offers the entire information of the pair correlation functions in Fourier space, comprising naturally the one-dimensional information on the static structure factor $S(Q)$, the present data with the coherent INS results[7] establish a complete and accurate experimental report of the dynamics and static properties of amorphous water ice structures.

*koza@ill.fr

[1] O. Mishima, L. D. Calvert, and E. Whalley, Nature (London) **310**, 393 (1984).

[2] H. Schober, M. M. Koza, A. Tolle, C. Masciovecchio, F. Sette, and F. Fujara, Phys. Rev. Lett. **85**, 4100 (2000).

[3] M. M. Koza, H. Schober, B. Geil, M. Lorenzen, and H. Requardt, Phys. Rev. B **69**, 024204 (2004).

[4] D. D. Klug, E. Whalley, E. C. Svensson, J. H. Root, and V. F.

Sears, Phys. Rev. B **44**, 841 (1991).
[5] H. Schober, M. M. Koza, A. Toelle, F. Fujara, C. A. Angell, and R. Boehmer, Physica B **241-243**, 897 (1997).
[6] M. M. Koza, B. Geil, H. Schober, and F. Natali, Phys. Chem. Chem. Phys. **7**, 1423 (2005).
[7] M. M. Koza, Phys. Rev. B **78**, 064303 (2008).
[8] O. Yamamuro, Y. Madokoro, H. Yamasaki, T. Matsuo, I. Tsukushi, and K. Takeda, J. Chem. Phys. **115**, 9808 (2001).
[9] E. L. Gromnitskaya, O. V. Stal'gorova, V. V. Brazhkin, and A. G. Lyapin, Phys. Rev. B **64**, 094205 (2001).
[10] O. Andersson and H. Suga, Phys. Rev. B **65**, 140201(R) (2002).
[11] O. Mishima, Nature (London) **384**, 546 (1996).
[12] Y. Suzuki, Y. Takasaki, Y. Tominaga, and O. Mishima, Chem. Phys. Lett. **319**, 81 (2000).
[13] T. Loerting, C. Salzmann, I. Kohl, E. Mayer, and A. Hallbrucker, Phys. Chem. Chem. Phys. **3**, 5355 (2001).
[14] M. M. Koza, B. Geil, K. Winkel, C. Kohler, F. Czeschka, M. Scheuermann, H. Schober, and T. Hansen, Phys. Rev. Lett. **94**, 125506 (2005).
[15] M. M. Koza, T. Hansen, R. P. May, and H. Schober, J. Non-Cryst. Solids **352**, 4988 (2006).
[16] M. M. Koza, R. P. May, and H. Schober, J. Appl. Crystallogr. **40**, s517 (2007).
[17] M. M. Koza, T. Hansen, R. P. May, and H. Schober, Proceedings of the SKIN 2007—International Symposium on Time-Resolved Processes in Condensed Matter, Goettingen, 2007 (unpublished).
[18] M. Scheuermann, B. Geil, K. Winkel, and F. Fujara, J. Chem. Phys. **124**, 224503 (2006).
[19] M. M. Koza, H. Schober, S. F. Parker, and J. Peters, Phys. Rev. B **77**, 104306 (2008).
[20] A. K. Garg, Phys. Status Solidi A **110**, 467 (1988).
[21] M. M. Koza, H. Schober, T. Hansen, A. Tolle, and F. Fujara, Phys. Rev. Lett. **84**, 4112 (2000).
[22] M. Koza, H. Schober, A. Toelle, F. Fujara, and T. Hansen, Nature (London) **397**, 660 (1999).
[23] S. W. Lovesey, *Theory of Neutron Scattering from Condensed Matter* (Oxford Science, Oxford, UK, 1984).
[24] G. L. Squires, *Introduction to the Theory of Thermal Neutron Scattering* (Dover, Mineola, NY, 1996).
[25] M. Krisch and F. Sette, Top. Appl. Phys. **108**, 317 (2007).
[26] J. M. Perez-Mato, M. Aroyo, J. Hlinka, M. Quilichini, and R. Currat, Phys. Rev. Lett. **81**, 2462 (1998).
[27] E. L. Gromnitskaya, O. V. Stal'gorova, A. G. Lyapin, V. V. Brazhkin, and O. B. Tarutin, JETP Lett. **78**, 488 (2003).
[28] C. A. Tulk, R. Hart, D. D. Klug, C. J. Benmore, and J. Neuefeind, Phys. Rev. Lett. **97**, 115503 (2006).
[29] K. Winkel, M. S. Elsaesser, E. Mayer, and T. Loerting, J. Chem. Phys. **128**, 044510 (2008).
[30] F. Sette, G. Ruocco, M. Krisch, U. Bergmann, C. Masciovecchio, V. Mazzacurati, G. Signorelli, and R. Verbeni, Phys. Rev. Lett. **75**, 850 (1995).
[31] G. Ruocco, F. Sette, M. Krisch, U. Bergmann, C. Masciovecchio, and R. Verbeni, Phys. Rev. B **54**, 14892 (1996).
[32] F. Sette, G. Ruocco, M. Krisch, C. Masciovecchio, R. Verbeni, and U. Bergmann, Phys. Rev. Lett. **77**, 83 (1996).
[33] F. Sacchetti, J. B. Suck, C. Petrillo, and B. Dorner, Phys. Rev. E **69**, 061203 (2004).
[34] G. Monaco, A. Cunsolo, G. Ruocco, and F. Sette, Phys. Rev. E **60**, 5505 (1999).
[35] C. Y. Liao, S. H. Chen, and F. Sette, Phys. Rev. E **61**, 1518 (2000).
[36] M. Krisch *et al.*, Phys. Rev. Lett. **89**, 125502 (2002).
[37] M. Guthrie, C. A. Tulk, C. J. Benmore, and D. D. Klug, Chem. Phys. Lett. **397**, 335 (2004).
[38] M. M. Koza, Ph.D. thesis, Technische Universität Darmstadt, 2001.
[39] J. S. Tse, D. D. Klug, C. A. Tulk, E. C. Svensson, I. Swainson, V. P. Shpakov, and V. R. Belosludov, Phys. Rev. Lett. **85**, 3185 (2000).
[40] O. S. Subbotin, V. R. Belosludov, T. M. Inerbaev, R. V. Belosludov, and Y. Kawazoe, Comput. Mater. Sci. **36**, 253 (2006).
[41] O. S. Subbotin and V. R. Belosludov, J. Struct. Chem. **47**, S61 (2006).
[42] T. Strassle, S. Klotz, G. Hamel, M. M. Koza, and H. Schober, Phys. Rev. Lett. **99**, 175501 (2007).
[43] E. L. Gromnitskaya, O. V. Stal'gorova, and V. V. Brazhkin, JETP **85**, 109 (1997).
[44] A. G. Lyapin, O. V. Stal'gorova, E. L. Gromnitskaya, and V. V. Brazhkin, JETP **94**, 283 (2002).
[45] O. Mishima and H. E. Stanley, Nature (London) **396**, 329 (1998).
[46] H. E. Stanley, S. V. Buldyrev, M. Canpolat, O. Mishima, M. R. Sadr-Lahijanin, A. Scala, and F. W. Starr, Phys. Chem. Chem. Phys. **2**, 1551 (2000).
[47] P. G. Debenedetti, J. Phys.: Condens. Matter **15**, R1669 (2003).
[48] H. E. Stanley, S. V. Buldyrev, and N. Giovambattista, Physica A **342**, 40 (2004).
[49] H. E. Stanley, P. Kumar, L. Xu, Z. Yan, M. Mazza, S. V. Buldyrev, S.-H. Chen, and F. Mallamace, Physica A **386**, 729 (2007).
[50] H. E. Stanley, P. Kumar, G. Franzese, L. Xu, Z. Yan, M. Mazza, S. V. Buldyrev, S.-H. Chen, and F. Mallamace, Eur. Phys. J. Spec. Top. **161**, 1 (2008).